Chemical Engineering Science, Vol. 46, No. 1, pp. 113–121, 1991.
Printed in Great Britain.

0009–2509/91 $3.00 + 0.00

DIFFUSE-REFLECTANCE FTIR SPECTROSCOPY FOR KINETIC AND MECHANISTIC STUDIES OF CO_2 HYDROGENATION IN A CONTINUOUS RECYCLE REACTOR

M. R. PRAIRIE, J. G. HIGHFIELD and A. RENKEN†
Swiss Federal Institute of Technology, Lausanne, CH-1015, Switzerland

(*Received* 21 *July* 1989; *accepted for publication* 17 *January* 1990)

Abstract—The advantage of coupling a diffuse-reflectance infrared cell with a continuous-feed recycle reactor for *in situ* kinetic and mechanistic studies is illustrated in the study of CO_2 methanation over Ru/TiO_2. From transient and steady-state experiments, metal-adsorbed CO is identified as a major reaction intermediate and at 120°C occupies approximately 40% of the available ruthenium surface, while methane formation proceeds at a turnover frequency of $2.8 \times 10^{-3}\ s^{-1}$. In contrast, CO methanation is totally hindered under the same conditions. A simple kinetic model is proposed to account for the main trends observed. For CO_2 methanation, the temperature insensitivity of adsorbed CO coverage is interpreted on the basis of a generalized (two-stage) intermediate supply/consumption mechanism involving the reverse water-gas shift reaction.

INTRODUCTION

In situ infrared spectroscopy has been used for many years in the study of catalysis for identifying adsorbed intermediates and their relationship to the gas phase for an enormous variety of reaction, adsorption, and desorption systems. Until recently, such experiments have been carried out in the transmission mode where a small continuous reactor (i.e., IR cell) contains a very thin, pressed wafer of the catalyst through which IR radiation is directed. In this arrangement, the reaction mixture enters the IR cell and is somehow directed around the catalyst wafer in a single-pass operation. This configuration often leads to internal and external transport limitations and completely uncharacterized gas mixing (Prairie *et al.*, 1988; Kaul and Wolf, 1985). Furthermore, reliable information on how the gas composition relates to the adsorbate distribution seen by IR can only be obtained in the extreme of very low conversions, i.e., differential operation. To overcome some of these problems, Vannice *et al.* (1979) reported an elegant cell design in which the flowing gas mixture is forced through the pores of the pressed wafer, thereby greatly reducing the problem of diffusion and allowing the wafer to be realistically modeled as an ideal differential or integral reactor. However, this design places limitations on allowable total flow rates to avoid breaking the delicate catalyst wafer.

Many of the problems which plague the transmission arrangement can be avoided altogether by employing Diffuse-Reflectance Spectroscopy (DRS) which was recently introduced by Hamadeh *et al.* (1984) for catalytic studies. The main advantages of DRS, or Diffuse-Reflectance Infrared Fourier Transform Spectroscopy (DRIFTS) when used in a Fourier transform spectrometer, stem from the use of the catalyst as a powder bed rather than as a pressed wafer. First, the often tedious, time-consuming process of pellet pressing is unnecessary. Second, since modern, commercially available DRIFTS cells are designed so that reactor gas flows directly through the powder bed, the bed can usually be characterized as an integral or differential reactor. The only mass transport concerns are those of diffusion into the catalyst grains, if a porous material is used, and external transport to the grains. Also, DRIFTS offers certain spectroscopic advantages relative to transmission IR spectroscopy. Scattering which diminishes high-wavenumber throughout in transmission is not a problem, the workable spectral window is extended in the region of strong absorbance bands (typical of oxide supports) and DRIFTS shows a relative enhancement of overtone and combination bands which can be used to advantage when fundamentals are too broad and strong for analytical purpose (Highfield and Bowen, 1989).

Unfortunately, DRIFTS also has disadvantages, the most important being axial thermal gradients through the powder bed. This arises from the optical constraints of the reflectance mode, which require that the sample bed be heated from below since the upper surface must be open to the infrared radiation. Also, powders are notoriously poor thermal conductors. Temperature gradients can be substantially reduced by using a bed which is as small as possible, its minimum size ultimately limited by optical sensitivity factors, i.e., the penetration depth of the IR beam (typically 1–2 mm) and its diameter. Unfortunately, beds of this size exhibit very low catalytic activities, often extending beyond analytical sensitivity limits for gas-phase analysis. Ventner and Vannice (1988) have

†Author to whom correspondence should be addressed.

addressed similar problems for a commercially available DRIFTS cell, but much work is still needed in this area.

The objective of this paper is to describe a novel reactor design by which poor mixing is overcome through the use of an external recycle loop which contains a DRIFTS cell in addition to a fixed-bed catalytic reactor. In this way it is possible to couple all the advantages of *in situ* DRIFTS with a well-mixed system that permits meaningful studies at normal operating conditions, including high conversion.

Very few references to the use of external recycle loops with catalytic IR cells can be found in the literature. In one study, Kaul and Wolf (1986) used external recycling, with a recycle ratio of 50, to attenuate spatial temperature fluctuations found on a pressed wafer during an infrared study of ethylene oxidation. This work emphasizes the possible importance of thermal transport problems and their relation to gas flow characteristics. Such problems would be further reduced by using a powdered-bed in place of a pressed wafer, hence reducing thermal transfer between discrete catalyst particles relative to the rate of convective heat removal by the flowing gas. In an earlier work, Tamura (1978) employed an external recycle IR reactor for a batch study. Our design is the first to use an infrared cell and a conventional fixed-bed reactor linked together via an external recycle loop. Arranged as such, the infrared cell can be regarded as a window into the reactor, providing a view of the catalyst surface at normal operating conditions.

The value of such a configuration is illustrated via a transient and steady-state study of CO_2 methanation:

$$CO_2 + 4H_2 \rightarrow CH_4 + 2H_2O \qquad (1)$$

on titania supported ruthenium. This reaction was chosen for several reasons. First, it is known to be interesting from the point of view of infrared spectroscopy (Solymosi *et al.*, 1981b) and second, there still remain some unanswered questions concerning its mechanism. On supported noble metal catalysts, CO_2 and hydrogen mixtures produce metal-adsorbed CO, as has been proved by IR spectroscopy (Henderson and Worley, 1985; Kellner and Bell, 1981; Solymosi *et al.*, 1981a, b, 1985), and methane as the major product (Henderson and Worley, 1985; Solymosi *et al.*, 1981a, b; Weatherbee and Bartholomew, 1984). The adsorbed CO is thought to be a reaction intermediate which dissociates to form adsorbed oxygen and carbon, which is eventually hydrogenated, as in CO hydrogenation chemistry, to form methane (Henderson and Worley, 1985). Concentrations of adsorbed CO during CO_2 methanation are much lower than those encountered at the same conditions during CO hydrogenation (Solymosi *et al.*, 1981a), possibly explaining why the CO_2 reaction proceeds at temperatures much lower than those necessary for the analogous reaction with CO (Henderson and Worley, 1985). Finally, adsorbed CO does not form via simple CO_2 dissociation; hydrogen is required (Goodman *et al.*, 1984; Henderson and Worley, 1985; Solymosi and Kiss, 1985), which is retained on the surface even near saturation levels of CO coverage (Cant and Bell, 1982), possibly because both reactants may be adsorbed on the same site (Dalla Betta and Shelef, 1977; Henderson and Worley, 1985; Solymosi *et al.*, 1981a). Some questions still remain, concerning (1) the high selectivity for methane, (2) the mechanism by which the concentration of adsorbed CO remains low and (3) the mechanism by which CO_2, in the presence of H_2, is converted to adsorbed CO.

EXPERIMENTAL

Apparatus

A schematic diagram of the experimental set-up is shown in Fig. 1. The heart of the installation is a fixed-bed reactor which is directly coupled to the DRIFTS cell via an external recycle loop. Two banks of mass flow controllers supply reactants and diluent (Ar) to the reactor via a micro-volume four-way valve, across which the differential pressure is maintained at zero. Oxygen impurity was removed from the feed gases (99.9995% Ar, 99.998% H_2, 99.995% CO_2, 99.998% CO, Carbagas) using on-line indicating oxygen traps (Oxisorb, < 0.1 ppm O_2). Effluent from the reactor was sampled continuously through a two-stage pressure reduction valve into a Balzers QMG 420 quadrupole mass spectrometer operating at 1.2×10^{-7} mbar. The mass spectrometer was calibrated for methane in the range of 1–30 mol% at $m/e = 15$. The reactor is controlled at 0.4 bar overpressure with a back-pressure regulator, thus eliminating the effects of small pressure fluctuations introduced by the recycle pump.

The recycle pump is of the oscillating membrane type, having an internal volume of 1 cm^3, and at 1 bar and negligible pressure drop has a stated pumping rate of 15 l/min. Under the conditions of high pressure drop imposed by the catalyst bed, DRIFTS cell, and tubing, a recycle rate of 1800 ml/min is achieved (all flow rates in ml/min are referenced to 1 bar, 22°C). To a good approximation, ideal mixing behavior is approached for recycle ratios greater than 25 (provided limited reaction conversion, $< 2\%$ per pass), leading to a practical upper limit of 70 ml/min for the total feed flow rate in this case.

A water trap (20 ml glass U-tube) was introduced into the recycle loop and maintained at a chosen temperature with refrigerated ethanol to control the steady-state water concentration and to avoid liquid water accumulation in the recycle loop. In most cases, the trap was maintained at -30°C corresponding to a partial pressure of water in the recirculating gas phase equal to 280 ppm. The effectiveness of the water trap was verified for operating temperatures up to 160°C when the rate of water production was approximately 2 μmol $H_2O\ s^{-1}$. Both the infrared spectrometer and the on-line mass spectrometer were used for monitoring changes in the ambient water vapor level.

The fixed bed reactor consists of a stainless steel Nupro filter holder (part no. 2F-MM) which has

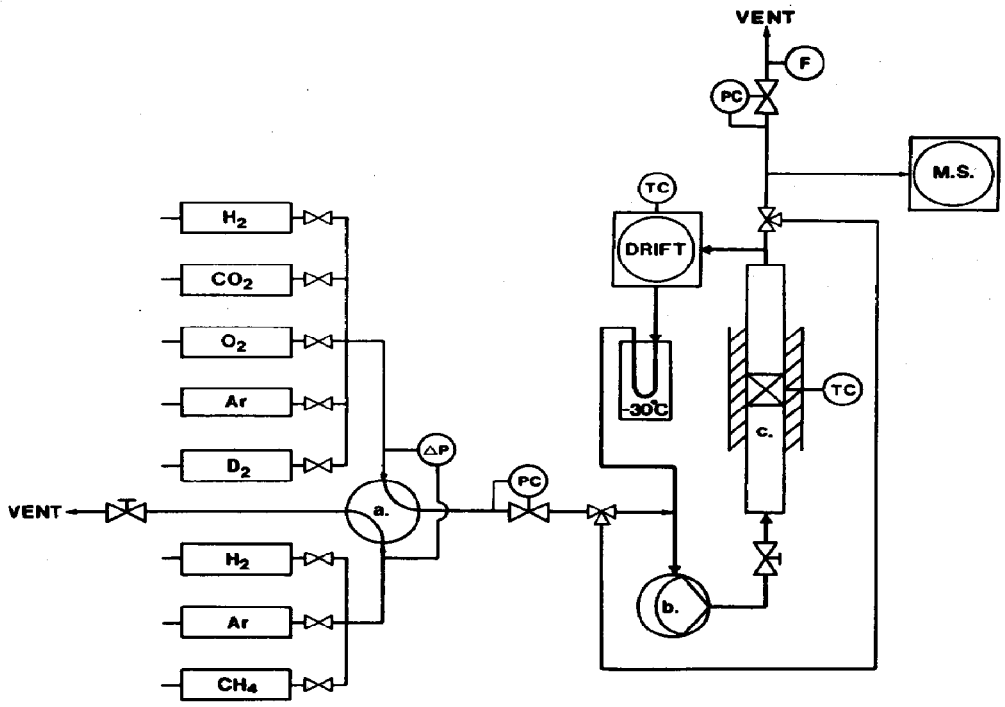

Fig. 1. Schematic layout of experimental apparatus. (a) Four-way switching valve. (b) Recirculation pump. (c) Heated fixed-bed tubular reactor.

internal dimensions of 10 mm dia., 13 mm length. Catalyst replaces the original filter and is held in place between two stainless steel screens (7 μm pores) and quartz wool. A 0.5 mm stainless steel jacketed thermocouple is located in the center of the bed and is used for temperature control. This mini-reactor is wrapped with heating tape and is well insulated.

Infrared spectra from 4000 to 800 cm^{-1} were obtained with a Bomem DA3.002 FTIR spectrometer equipped with a Harrick DRA-2CO DRIFT accessory and a short range HgCdTe detector. All spectra were recorded at 8 cm^{-1} resolution (co-adding 20 interferograms) and converted to relative reflectance against a pure KBr reference. Acquisition of each spectrum required 6 s. A Harrick HVP vacuum chamber cover with NaCl windows and a homemade base of our own design comprised the DRIFT cell. The new base was built primarily to improve heat transfer characteristics across the bed. Some consideration was also given in the new design to flow and mixing properties.

Temperature gradients in the DRIFTS powder bed were monitored with two 0.5 mm stainless steel sheathed thermocouples, one located deep in the bed and the other in its center, just below the irradiated upper surface. At 200°C, the temperature difference between the two thermocouples never exceeded 3°C, even when flowing greater than 1 l/min of gas directly through the bed. Temperature in the sample-bed was controlled using a Eurotherm 815 PID controller, based on the center thermocouple.

Excellent backmixing for the entire recirculation system was verified via step-response tracer experiments which produced exponential response curves. A residence time, τ, of 1.7 min was observed when 50 ml/min was used as the feed rate to the recirculation system. This feed rate corresponds to a recycle ratio of about 36.

Methodology

The system was loaded with 670 mg (100 mg in the DRIFT cell) of Ru/TiO_2 whose preparation and properties are described by Thampi *et al.* (1987) and listed in Table 1 along with nominal experimental conditions. The catalyst was first oxidized at 210°C in flowing O_2 (20% in Ar) for 1 h before being reduced in flowing H_2 (20% in Ar) at 210°C for 1 h and then cooled to 120°C before being exposed to a steady feed mixture of 20 ml/min H_2 and 10 ml/min CO_2 (referred to as the standard mixture) and then allowed to stabilize overnight. These conditions yielded a methane formation rate of 0.17 μmol/s and an H_2 conversion of 5%. Between 100°C and 200°C, the catalyst did not deactivate and no products other than methane and water were observed.

Four transient isothermal (120°C) experiments were performed where the reactor feed composition was changed in a stepwise manner. One of these experiments compares CO methanation with CO_2 methanation at identical conditions. In each case, DRIFT spectra were recorded at 3 min intervals along with continuous mass spectrometric analysis of

Table 1. Catalyst properties and standard operating conditions

Catalyst	
Mass	100 mg in DRIFTS cell 570 mg in fixed-bed reactor
Support	Degussa P-25 TiO_2
Ru loading	3.8% by mass
BET surface area	55 m^2/g
Dispersion	0.5 by H_2 chemisorption
Experimental parameters	
Flow rate	50 ml/min (22°C, 1 bar)
Recycle ratio	36
Standard feed mixture	20 ml/min H_2, 10 ml/min CO_2, 20 ml/min Ar
Standard temperature	120°C
Methane production rate at standard conditions	0.25 μmol/s/g at 5% H_2 conversion

methane ($m/e = 15$), H_2($m/e = 2$), water ($m/e = 18$), and CO_2 ($m/e = 44$). Spectra are presented as relative reflectance ratioed against the spectrum of the clean catalyst after reduction in hydrogen. In some cases, integral data of infrared absorbance bands are presented. These data were obtained by first transforming relative reflectance spectra into the Kubelka–Munk form and then making the appropriate baseline corrections before numerical integration. Integrated band intensities in Kubelka–Munk units are analogous to integrated absorbance bands in the transmission mode, and are linearly related to concentration over a certain reflectance range (Kortüm, 1969). The feed mixtures employed for the switching experiments are listed in Table 2.

One series of steady-state data are presented which show the effects of temperature on methane production rate and surface-adsorbed species. At each of six temperatures ranging between 120°C and 172°C, the effluent methane concentration was determined using the calibrated mass spectrometer. Reaction rates and reactant concentrations were calculated using a material balance for an ideal continuous stirred-tank reactor (CSTR) taking into account that water was being trapped in the system. Hydrogen and CO_2 partial pressures were maintained constant at 390 mbar and 88 mbar, respectively, throughout the series by adjusting feed rates according to conversion levels.

In another group of steady-state experiments, the dependence of reaction rate and infrared spectra was determined as a function of water concentration. Water levels were varied by changing the trap temperature for isothermal reactor operation at 165°C, 21 mol% H_2, and 13 mol% CO_2. Relative water concentrations were determined with the mass spectrometer at $m/e = 18$.

RESULTS AND DISCUSSION

Transient experiments

Figure 2 shows reflectance spectra for transient experiment A between 1200 and 2200 cm^{-1}. The lowermost spectrum is that for the system at steady-state and standard conditions. The absorbance band with its maximum absorbance near 2016 cm^{-1} only appears if both CO_2 and H_2 are present on the catalyst and is due to metal-adsorbed CO ($CO_{(a)}$), possibly on the same site with one or more hydrogen atoms (Dalla Betta and Shelef, 1977; Kellner and Bell, 1981; Solymosi *et al.*, 1981a, b). As will be discussed later, the band shifts to lower wavenumber with lower intensity, i.e., with lower surface coverage. The two bands at 1555 and 1360 cm^{-1} are due to support-based carbonates, bicarbonates, and/or formates

Table 2. Feed mixtures for transient experiments

Experiment	Feed initially	Switched to
A	Standard mixture (40% H_2 and 20% CO_2 balance Ar, 50 ml/min total flow rate)	50 ml/min Ar
B	Standard mixture	20 ml/min H_2 30 ml/min Ar
C	10 ml/min CO 20 ml/min H_2 20 ml/min Ar	20 ml/min H_2 30 ml/min Ar
D	Standard mixture	50 ml/min Ar (18 min) then switched to 20 ml/min H_2 30 ml/min Ar

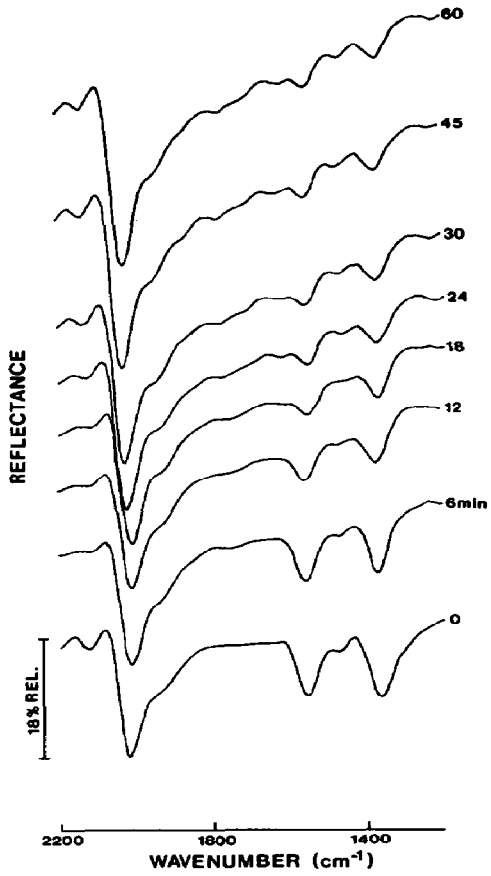

Fig. 2. *In situ* DRIFTS transient behavior of $CO_{(a)}$ at 120°C after switching from the standard mixture (40% H_2 and 20% CO_2) to pure Ar, experiment A.

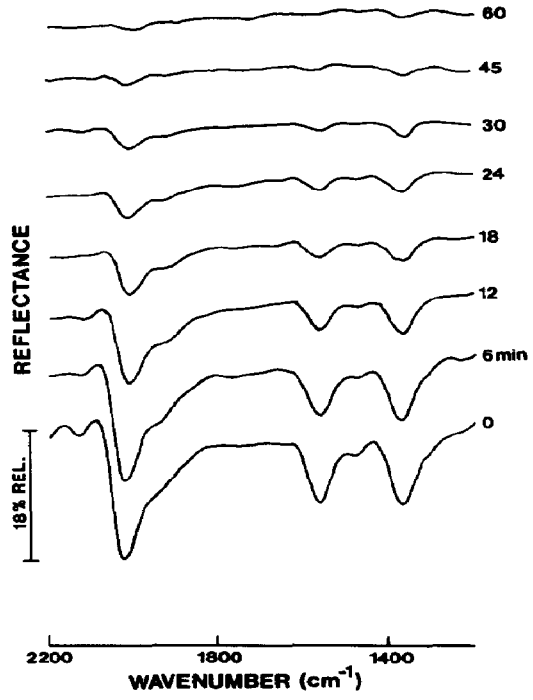

Fig. 3. *In situ* DRIFTS transient behavior of $CO_{(a)}$ at 120°C after switching from the standard mixture (40% H_2 and 20% CO_2) to 40% H_2, experiment B.

whose contribution to the overall reaction is still unclear (Henderson and Worley, 1985; Kellner and Bell, 1981; Solymosi *et al.*, 1981a). The series of spectra show that $CO_{(a)}$ coverage first dropped slightly and then increased with time while the carbonate/formate species disappeared uniformly. It is possible that these latter species migrate from the support to the metal where they contribute to the apparent overall increase in metal coverage by $CO_{(a)}$.

Figure 3 shows the transient progression of $CO_{(a)}$ and surface carbonate/formate during experiment B. Here, H_2 actively consumes $CO_{(a)}$ and the carbonate/formate bands disappear much more quickly than they do in argon alone. This suggests that support-stored carbonates and formates may be a source of methane, via $CO_{(a)}$, provided that hydrogen is available. Both experiments A and B show a uniform shift in absorbance frequency with changing surface coverage. The band appears at 2030 cm^{-1} for the highest coverage (60 min, expt. A), and near 1975 cm^{-1} as coverage approaches zero.

Integrals of the $CO_{(a)}$ absorbance envelope in Kubelka–Munk units for experiments A and B are shown in Fig. 4 along with transient reactor effluent composition. The figure clearly shows that adsorbed CO is a methanation intermediate, the integral difference between the two methane trajectories B and A being *roughly* equal to the amount of $CO_{(a)}$ stored on the catalyst at steady-state (i.e., before the switch to hydrogen). Exact correspondence is not expected for three reasons: (1) continuing adsorption from the gas phase artificially increases the integral; (2) surface carbon, a well-known CO methanation intermediate not easily seen by IR, increases the amount of methane produced attributable to $CO_{(a)}$ alone; and (3) support-stored carbonates and formates may also have contributed to the methane observed, albeit via adsorbed CO. The strange behavior of adsorbed CO during experiment A, where coverage first falls and then rises to a level greater then its initial steady-state level could be the result of dynamic interactions between the various mechanisms for $CO_{(a)}$ formation and consumption, and contributions from the gas phase.

Figure 5 shows what happens when CO is used instead of CO_2 before the feed mixture is switched to hydrogen (experiment C). The steady-state spectrum taken at time = 0 shows a large amount of metal-adsorbed CO (2047 cm^{-1}), gas-phase CO (2076 cm^{-1} and the shoulder on the $CO_{(a)}$ band), and gas-phase CO_2 (2350 cm^{-1}). Under these conditions no methane was detected in the gas phase, suggesting total inhibition by $CO_{(a)}$, which is a well-known phenomenon in Fischer–Tropsch chemistry on transition metals (e.g., Vannice, 1982). Interestingly, even though the metal surface was totally covered by $CO_{(a)}$, the continuous production of gas phase CO_2 suggests the

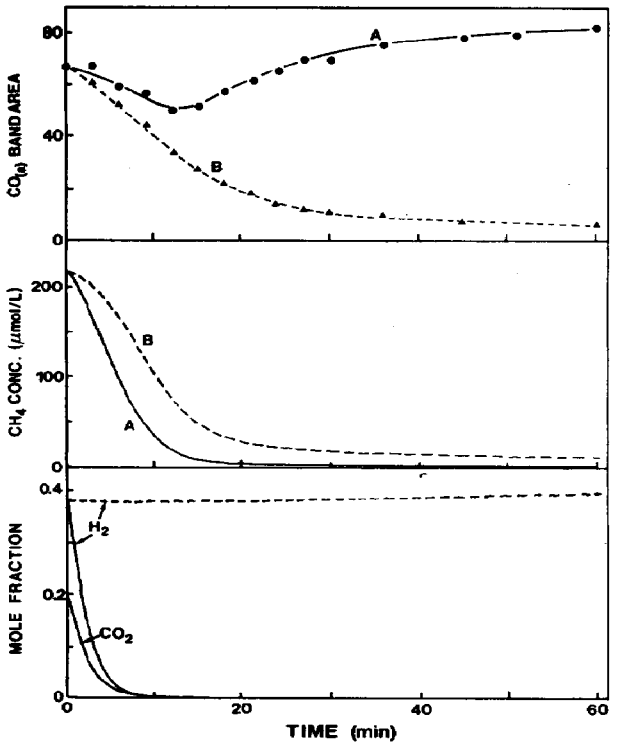

Fig. 4. Transient behavior of integrated $CO_{(a)}$ band area, methane, and reactant concentrations for experiments A (solid) and B (dashed).

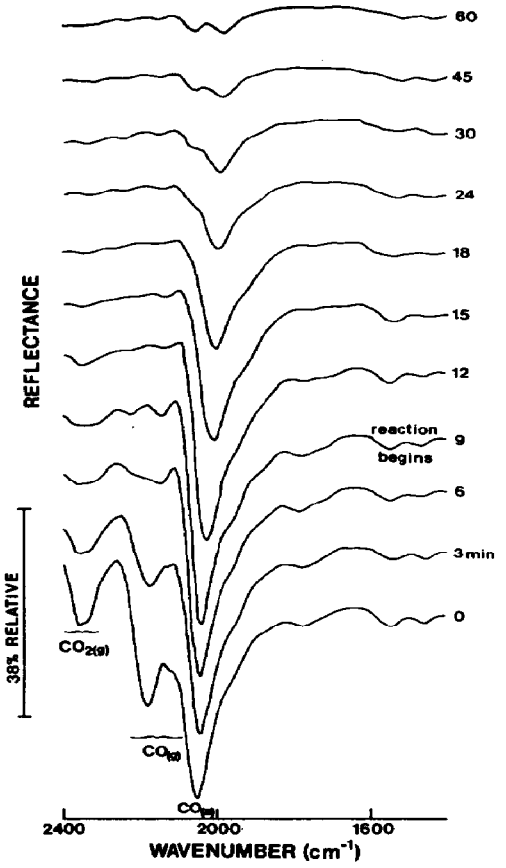

Fig. 5. *In situ* DRIFTS transient behavior at 120°C after switching from 40% H_2 and 20% CO to 40% H_2 in Ar, experiment C. The original steady-state spectrum at time zero shows metal-adsorbed CO, gas-phase CO, and gas-phase CO_2. Initially the reaction is inhibited and no methane is produced. Nine minutes after the switch methane production begins.

occurrence of the water-gas shift reaction. To verify this hypothesis, the temperature of the water trap was manipulated in order to change the gas-phase water concentration, the result being that the CO_2 concentration varied directly with water concentration. Due to the nature of the recycle system and water trap, the absolute water concentration in the reactor was never lower than approximately 280 ppm.

Gas-phase CO and CO_2 were purged from the reactor following the switch to H_2 in experiment C. During this time the surface coverage by adsorbed CO remained essentially unchanged as seen by the first four spectra in Fig. 5. Suddenly, around 9 min after the switch, methane was rapidly evolved and approximately 60 min later, the catalyst was practically devoid of any adsorbed CO. Apparently, in the absence of gas-phase CO, $CO_{(a)}$ was removed by the water-gas shift reaction and/or CO desorption to a coverage low enough for hydrogenation to take over, rapidly cleaning the surface and producing methane. No other hydrocarbons were detected by mass spectrometry during the methane burst.

These results are summarized in Fig. 6, which shows the methane concentration in the reactor effluent for experiment C in comparison to experiment D, which is simply a repetition of experiment A modified to include a switch to 40% H_2 after an 18 min purge in Ar. The elution curve for gas-phase CO for experiment C is also shown as a measure of the mixing dynamics of the system. The inset shows the

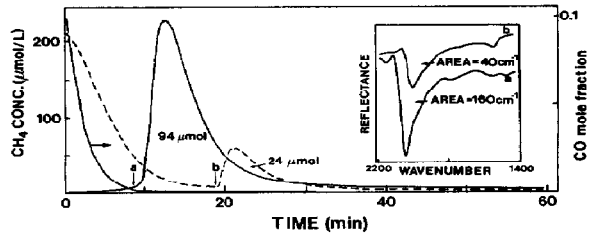

Fig. 6. Transient methane behavior for experiments C (solid) and D (dashed). Gas-phase CO concentration is also shown for experiment C. The inset shows reflectance spectra of adsorbed CO for experiments C and D at points a and b, respectively. Complete coverage of the active Ru surface corresponds to 94 μmol of adsorbed CO.

$CO_{(a)}$ band 9 min after the switch in experiment C (point a) and just before the switch to hydrogen in experiment D (point b). The methane produced during experiment C was 94 μmol. This quantity must correspond to the amount of CO on the catalyst giving rise to the absorbance band at point a, which

when integrated yields a value of 160 cm^{-1} in Kubelka–Munk units. Similarly, 24 μmol of methane were produced upon switching to hydrogen in experiment D, corresponding to the amount of $CO_{(a)}$ on the catalyst at point b and a Kubelka–Munk integral of 40 cm^{-1}. It is striking that the ratios of methane peaks and Kubelka–Munk integrals are identical at 0.25, providing strong evidence that under the conditions of experiment D, $CO_{(a)}$ was the major intermediate in methane formation.

If it is assumed that the amount of methane produced in experiment C corresponds to the amount of CO on the surface at complete coverage, then an estimate for the number of available ruthenium sites in the reactor is 94 μmol, corresponding to a metal dispersion of 0.4. This value is in reasonable agreement with the hydrogen chemisorption result of 0.5 (Thampi *et al.*, 1987). The assumption of a 1:1 correspondence between methane produced and adsorbed CO is justified since initially the reaction was totally hindered, indicating that the metal was completely covered by CO and that no other carbonaceous species that could form methane, such as adsorbed carbon, existed on the surface. Also, the spectra in Fig. 5 show that little carbonate or formate was present on the support during the experiment.

The equivalence between the methane ratio and the ratio of $CO_{(a)}$ integrated band intensities (=0.25) for experiments C and D suggests that little if any reactive carbonaceous species were accumulated on the catalyst during experiment D, and that a rate-determining step for the hydrogenation of adsorbed CO may be the dissociation process, possibly assisted by adsorbed hydrogen.

Going back to the steady-state level of $CO_{(a)}$ during CO_2 methanation at standard conditions, the bottom spectrum in Fig. 2. produces a Kubelka–Munk area of 67 cm^{-1}. From this and the result of experiment C, steady-state $CO_{(a)}$ coverage can be estimated: $\theta_{CO} = 67/160 = 0.4$. Clearly, CO_2 methanation is far from being hindered by an excessive accumulation of $CO_{(a)}$.

Steady-state experiments

A series of steady-state data were taken with 650 mg of the catalyst to determine the effects of temperature on the rate of methane formation and CO coverage. Data are shown in Arrhenius form in Fig. 7 for temperatures ranging from 120°C to 172°C at constant H_2 and CO_2 partial pressures, 390 mbar and 88 mbar, respectively. The observed rates correspond to turnover frequencies between 2.8×10^{-3} and 47×10^{-3} s^{-1}, calculated based on a metal dispersion of 0.4. These values are remarkably high relative to typical values for CO methanation, which is normally carried out at or above 250°C (Vannice, 1982) and generally superior to published values for CO_2 methanation, e.g., 194×10^{-3} s^{-1} for Ru/Al_2O_3 at 275°C (Solymosi *et al.*, 1981b), 150×10^{-3} s^{-1} on Rh/TiO_2 at 200°C (Solymosi *et al.*, 1981a), and 7.2×10^{-3} s^{-1} on Ru/SiO_2 at 225°C (Weatherbee and

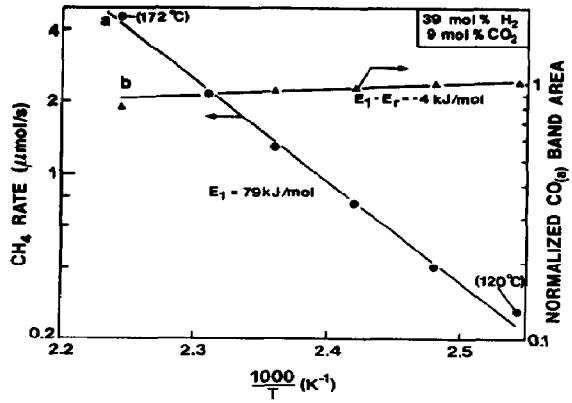

Fig. 7. Arrhenius plot of temperature dependence of methanation rate (a) and CO band area (b) at steady-state for 390 mbar H_2 and 88 mbar CO_2.

Bartholomew, 1984). The data show simple behavior for methane formation rate yielding an activation energy of 79 kJ/mol. Surface coverage by CO varies remarkably little with temperature, exhibiting an apparent activation energy of −4 kJ/mol.

Figure 8 shows how methane production rate and CO coverage depend on water concentration for steady-state operation at 165 °C. Both are suppressed by water, the effect appearing relatively more important for the overall reaction rate than for the quantity of adsorbed CO.

Interpretation

The transient and steady-state experiments described above have provided insight into the questions raised in the Introduction. The high selectivity for methane during CO_2 hydrogenation may simply result from the low levels of adsorbed CO ($\theta_{CO} \leqslant 0.5$) which are present during the reaction. It is intuitively obvious that if the adsorbed CO concentration is low, then on average these molecules will be further apart, thus rendering carbon–carbon bond formation and chain growth more difficult. In addition, it is a well-known fact of Fischer–Tropsch chemistry that higher temperatures and hence lower $CO_{(a)}$ coverage favor methane as the reaction product.

The experiments also suggest that CO coverage is controlled through the *reverse water-gas shift* (RWGS) reaction, as evidenced by the negative-order dependence of adsorbed CO on water vapor concentration. Here, the relevant form of the RWGS reaction involves adsorbed, rather than gas-phase, species and is written

$$CO_2 + 2H_{(a)} \underset{k_2}{\overset{k_1}{\rightleftharpoons}} CO_{(a)} + H_2O. \qquad (2)$$

Combining this reaction with a lumped expression for hydrogenation of $CO_{(a)}$ (including dissociation and $C_{(a)}$ hydrogenation processes),

$$CO_{(a)} + 6H_{(a)} \overset{k_r}{\rightarrow} CH_4 + H_2O_{(g)}, \qquad (3)$$

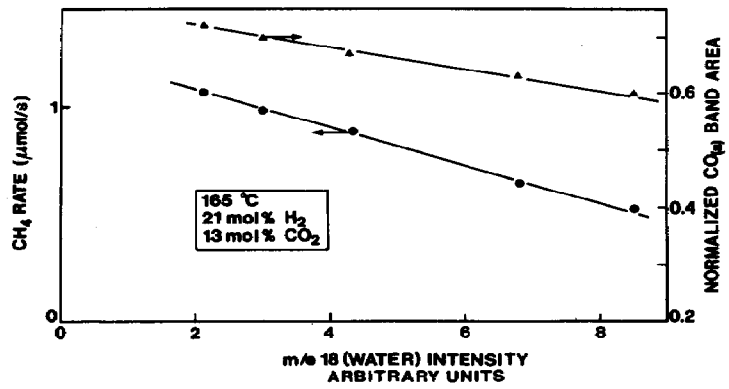

Fig. 8. Reaction rate and CO coverage dependence on steady-state water concentration at 165°C. Integral band areas are normalized with that observed at 120°C in the standard feed mixture.

one can easily obtain informative expressions for CO coverage θ_{CO}, and the methane formation rate, R_{CH_4}:

$$\theta_{CO} = \frac{k_1[CO_2]p_{H_2}^m}{k_2 p_{H_2O} + k_r p_{H_2}^n} \quad (4)$$

$$R_{CH_4} = k_r\theta_{CO}p_{H_2}^n = \frac{k_r k_1[CO_2]p_2^{m+n}}{k_2 p_{H_2O} + k_r p_{H_2}^n} \quad (5)$$

invoking the results of Cant and Bell (1982) that methanation shows a first-order dependence on $CO_{(a)}$, and that adsorbed hydrogen is in equilibrium with the gas phase (allowing rate dependencies on hydrogen to be expressed as powers of the hydrogen partial pressure, m and n, for the reverse shift and methanation steps, respectively). In these equations, $[CO_2]$ is the concentration of active CO_2, whether it be in the gas or on the support and k_1, k_2, and k_r are temperature-dependent rate coefficients. The assumption of hydrogen equilibration is reasonable since CO surface coverage never exceeds 0.5, and unlike CO methanation, CO_2 methanation does not exhibit any form of inhibition except that caused by water, a feature exhibited by the model and shown experimentally in Fig. 8.

When the reaction rate is very low and essentially all of the water is trapped, the reverse step in reaction (2) can be neglected, reducing eqs (4) and (5) to:

$$\theta_{CO} = \frac{k_1}{k_r}[CO_2]p_{H_2}^{m-n} \quad (6)$$

and

$$R_{CH_4} = k_1[CO_2]p_{H_2}^m. \quad (7)$$

According to this argument, θ_{CO} should exhibit an apparent activation energy which is the difference between that for the forward reaction in eq. (2) and that for $CO_{(a)}$ hydrogenation, eq. (3). Similarly, the observed activation energy for the overall formation of methane should be the activation energy of the forward part of the reverse WGS reaction (E_1) equal to 79 kJ/mol on Ru/TiO_2. The activation energy for $CO_{(a)}$ hydrogenation is then simply given by $E_1 - E_r = 79 - (-4)$ kJ/mol = 83 kJ/mol, which is identical to the finding of Cant and Bell (1982) for Ru/SiO_2. A more general development of eqs (4) and (5) explicitly including temperature and hydrogen pressure dependencies on the hydrogen adsorption equilibrium does not affect these qualitative conclusions.

CONCLUSIONS

By virtue of the separate DRIFTS cell and fixed-bed reactor, it is possible to minimize the amount of catalyst in the IR cell (to reduce heat transfer problems) and still maintain significant rates of product formation. The system is ideal for determining steady-state kinetics over a wide range of reactant partial pressures, including the determination of quantitative relationships between adsorbate concentration, feed composition and reaction rate. The system is also amenable to transient experiments, which are important for model identification and for titrations useful in relating adsorbate concentrations to IR band intensities. Increased flexibility in experimental design results from the freedom to use significant amounts of catalyst, the ability to determine meaningful kinetic parameters over a wide range of conversions, the ability to quantitatively study adsorbed intermediates via *in situ* infrared spectroscopy, together with simplified and accurate mathematical data interpretation (i.e., ideal continuous stirred tank, CSTR, equations).

The primary goal of this work to demonstrate the usefulness of the external recycle, fixed-bed/DRIFTS cell reactor for heterogeneous catalysis studies. In doing so, we were able to clarify several aspects relating to CO_2 methanation on supported Ru. Further work using this reactor to more thoroughly characterize the steady-state kinetics and dynamic behavior of the reaction is in progress.

Acknowledgements—Funding for this work was provided by the Swiss National Foundation. We are grateful to Dr. K. R. Thampi for providing the catalyst.

NOTATION

E_1	activation energy for forward step in the RWGS reaction
E_r	activation energy for $CO_{(a)}$ hydrogenation step
k_1	rate coefficient for forward step of the RWGS reaction
k_2	rate coefficient for reverse step of the RWGS reaction
k_r	rate coefficient for $CO_{(a)}$ hydrogenation step
p_{H_2}	hydrogen partial pressure
R_{CH_4}	methane formation rate
θ_{CO}	fractional surface coverage by CO

REFERENCES

Cant, N. W. and Bell, A. T., 1982, Studies of carbon monoxide hydrogenation over ruthenium using transient response techniques. *J. Catal.* **73**, 257–271.

Dalla Betta, R. A. and Shelef, M., 1977, Heterogeneous methanation: *in situ* infrared spectroscopic study of Rh/Al_2O_3 during hydrogenation of CO. *J. Catal.* **48**, 111–119.

Goodman, D. W., Peebles, D. E. and White, J. M., 1984, CO_2 dissociation on rhodium: measurement of the specific rates on Rh (111). *Surface Sci.* **140**, L239–L243.

Hamadeh, I. M., King, D. and Griffiths, P. R., 1984, Heatable–evacuable cell and optical system for diffuse reflectance FT-IR spectrometry of adsorbed species. *J. Catal.* **88**, 264–272.

Henderson, M. A. and Worley, S. D., 1985, An infrared study of the hydrogenation of carbon dioxide on supported rhodium catalysts. *J. phys. Chem.* **89**, 1417–1423.

Highfield, J. G. and Bowen, P., 1989, Diffuse-reflectance Fourier-transform infrared spectroscopic studies of the stability of aluminum nitride powder in an aqueous environment. *Analyt. Chem.* (in press).

Kaul, D. J. and Wolf, E. E., 1985, FTIR studies of surface reaction dynamics. *J. Catal.* **91**, 216–230.

Kaul, D. J. and Wolf, E. E., 1986, Transient FTIR studies of multiplicities, oscillations, and reaction non-uniformities during CO and ethylene oxidation on supported Pt and Pd catalysts. *Chem. Engng Sci.* **41**, 1101–1107.

Kellner, C. S. and Bell, A. T., 1981, Infrared studies of carbon monoxide hydrogenation over alumina-supported ruthenium. *J. Catal.* **71**, 296–307.

Kortüm, G., 1969, *Reflectance Spectroscopy.* Springer-Verlag, Berlin.

Prairie, M. R., Cho, B. K., Oh, S. H., Shinouskis, E. J. and Bailey, J. E., 1988, Steady-state and transient studies of carbon monoxide oxidation on alumina-supported rhodium via transmission infrared spectroscopy. *Ind. Engng Chem. Res.* **27**, 1396–1407.

Solymosi, F. and Kiss J., 1985, Impurity effects in the adsorption and dissociation of CO_2 on Rh. *Surface Sci.* **149**, 17–32.

Solymosi, F., Erdöhelyi, A. and Bànsàgi, T., 1981a, Methanation of CO_2 on supported rhodium catalyst. *J. Catal.* **68**, 371–382.

Solymosi, F., Erdöhelyi, A. and Kocsis, M., 1981b, Methanation of CO_2 on supported Ru catalyst. *J. chem Soc., Faraday Trans. 1* **77**, 1003–1012.

Solymosi, F., Erdöhelyi, A. and Lancz, M., 1985, Surface interaction between H_2 and CO_2 over palladium on various supports. *J. Catal.* **95**, 567–577.

Tamura, K., 1978, *Dynamic Heterogeneous Catalysis*, pp. 96–99. Academic Press, London.

Thampi, K. R., Kiwi, J. and Grätzel, M., 1987, Methanation and photo-methanation of carbon dioxide at room temperature and atmospheric pressure. *Nature* **327**, 506–508.

Vannice, M. A., 1982, *Catalysis: Science and Technology* (Edited by Anderson, J. R. and Boudart, M.), Vol. 3, pp. 139–198. Springer-Verlag, New York.

Vannice, M. A., Moon, S. H., Twu, C. C. and Wang, S.-Y., 1979, A design for a combined infrared cell/differential single-pass reactor. *J. Phys. E: Sci. Instrum.* **12**, 849–852.

Ventner, J. J, and Vannice, M. A., 1988, Modifications of a diffuse reflectance cell to allow the characterization of carbon-supported metals by DRIFTS. *Appl. Spectrosc.* **42**, 1096–1103.

Weatherbee G. D. and Bartholomew, C. H., 1984, Hydrogenation of CO_2 on group VIII metals. *J. Catal.* **87**, 352–362.